ACS Photonics

Article

pubs.acs.org/journal/apchd5

Nonimaging Optical Gain in Luminescent Concentration through Photonic Control of Emission Étendue

Yufei Shen,[†,‡] Yufei Jia,[†] Xing Sheng,[§] Ling Shen,[∥] John A. Rogers,[§] and Noel C. Giebink*[,†]

Departments of [†]Electrical Engineering and [‡]Physics, The Pennsylvania State University, University Park, Pennsylvania 16802, United States

[§]Department of Materials Science and Engineering and Frederick Seitz Materials Research Laboratory, University of Illinois at Urbana−Champaign, Urbana, Illinois 61801, United States

[∥]Department of Physics, College of Sciences, China University of Mining and Technology, Xuzhou, Jiangsu 221116, People's Republic of China

Supporting Information

ABSTRACT: Luminescent and nonimaging optical concentration constitute two fundamentally different ways of collecting and intensifying light. Whereas nonimaging concentrators based on reflective, refractive, or diffractive optics operate most effectively for collimated light, luminescent concentrators (LCs) rely on absorption, re-emission, and waveguiding to concentrate diffuse light incident from any direction. LCs have been explored in many different shapes and sizes but have so far been unable to exploit the power of nonimaging optics to further increase their concentration ratio because their emission is angularly isotropic. Here, we use a luminescent thin film bilayer to create sharply directed conical emission in an LC and derive a nonimaging optical solution to leverage this directionality for secondary geometric gain ranging up to an order of magnitude or higher. We demonstrate this concept experimentally using a custom compound parabolic optical element index-matched to the LC surface and show that it delivers three times more luminescent power to an opposing GaAs photovoltaic cell when the emission profile is conically directed than when it is isotropic or the nonimaging optic is absent. These results open up a significant and general opportunity to improve LC performance for a variety of applications including photovoltaics, photobioreactors, and scintillator-based radiation detection.

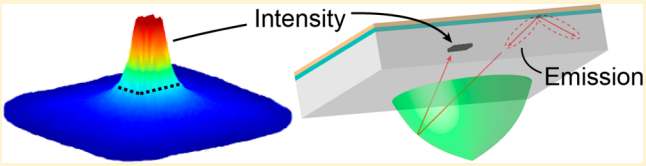

KEYWORDS: *luminescence, solar concentration, nonimaging optics, microcavity, spontaneous emission, photovoltaics*

The ability to concentrate light is fundamentally important in optics and plays a key role in applications ranging from solar energy conversion to high-energy radiation detection.[1−4] In general, light may be concentrated elastically (no change in photon energy) as in the case of geometric concentrators based on lenses, mirrors, and diffractive elements,[1,2] or it may be concentrated inelastically via a Stokes' shift through the process of luminescent concentration.[5,6]

Nonimaging optics is the basis for geometric concentrators that maximize radiative transfer by optimally transforming the incident optical étendue, that is, by converting between the spatial and the angular extent of light with minimal loss.[1,2] Nonimaging concentrators operate ideally by accepting light with limited angular extent (that is, range of impinging angles) and transforming it to fill the full 2π steradian half-space at the (smaller) output aperture. The resulting trade-off between maximum concentration ratio (CR_{max}) and acceptance angle (θ_{acc}) is set thermodynamically by conservation of étendue and embodied in the well-known sine law, $CR_{max} \propto (\sin \theta_{acc})^{-2}$ which, for example, requires geometric solar concentrators to track the Sun in order to reach high concentration ratio (CR > 100).[1−3]

Inelastic luminescent concentrators (LCs) operate differently by absorbing incident light and re-emitting it, Stokes' shifted to lower frequency, into the confined modes of a waveguide.[7−9] Owing to the entropy generated in the Stokes' shift, LCs can operate beyond the sine limit and attain high CR, independent of θ_{acc};[5,6] however, in practice they operate well below their thermodynamic potential due to nonunity luminescence quantum yield, reabsorption-based escape cone, and parasitic scattering optical losses.[7,8,10−14] To date, the fields of luminescent and nonimaging concentration have progressed largely independent of one another since the isotropic emission of traditional LCs offers little opportunity for secondary nonimaging optical gain.

Here, we provide a path to merge these two approaches by combining an LC architecture that enables highly directional emission together with a surface-mounted nonimaging optic and show that it increases the luminescent power delivered to a GaAs photovoltaic cell by more than a factor of 3. Optical modeling supports the observed improvement and indicates

Received: June 4, 2014
Published: July 18, 2014

that it can be maintained in large-area arrays that also benefit from a cooperative ray-recycling effect in which light rejected by one optic is accepted by another. These results point to a new opportunity at the intersection of luminescent concentration, photonics, and nonimaging optics to concentrate and otherwise manipulate incoherent, diffuse illumination.

OPPORTUNITY FOR NONIMAGING GAIN WITH DIRECTIONAL LUMINESCENCE

Various optical approaches have been explored to improve LC performance, including different LC shapes and fiber geometries,[15,16] wavelength selective mirrors to reduce escape-cone loss,[17,18] and patterned dye regions with and without primary lenses to reduce reabsorption.[19,20] Alternatively, the opportunity for secondary geometric gain of the luminescence itself was recognized early on,[21] where molding the edge of a typical LC slab in the form of a compound parabolic concentrator enables the output intensity to be increased by a factor $\beta = 1/\sin(90° - \theta_{crit})$ since the total internal reflection critical angle, θ_{crit}, naturally limits the angular extent of luminescence reaching the edge.[22] This enhancement is modest ($\beta \sim 1.3$) for a standard glass or acrylic LC in which $\theta_{crit} \sim 42°$ constitutes the only angular restriction; however, it is intuitively evident from sine law consideration that LCs with highly directional emission can achieve a much larger geometric boost if suitable nonimaging elements can be incorporated.

Figure 1 illustrates the comparison between a conventional LC with isotropic emission and a directional LC (DLC) where light emission peaks strongly at a single angle, θ_{em}, relative to the LC surface normal ($\theta_{em} > \theta_{crit}$). In the latter case shown in Figure 1b, a reflective nonimaging optic consisting of two offset parabaloids with symmetrically tilted axes is designed to redirect all waveguided luminescence to a surface-mounted solar cell. For luminescence restricted in the angular range $[\theta_1, \theta_2]$, the minimum size of the solar cell required to collect all of the guided light can be determined using the edge ray principle[1,2] together with the construction in Figure 1b to be $d_{cell} = d_{LC}(\tan\theta_2 - \tan\theta_1)$, where d_{LC} is the LC thickness. The geometric increase in concentration ratio per unit of illuminated solar cell area relative to the conventional case in Figure 1a is thus $\beta = 2/(\tan\theta_2 - \tan\theta_1) \approx 2\cos^2\theta_{em}/\Delta\theta_{em}$, where the approximate expression holds when θ_{em} lies midway between the angular limits and the difference between them $\Delta\theta_{em} = \theta_2 - \theta_1$ is small. It is evident from this expression that the geometric gain is maximized for highly directional emission (small $\Delta\theta_{em}$) and θ_{em} chosen just above the critical angle (that is, as small as possible); for emission confined in the range [44°, 56°] typical of the experimental data below, $\beta \sim 3.9$.

As in the classical compound parabolic concentrator (CPC) case, the derivation above holds rigorously in two dimensions (2D) but not in 3D when the optic in Figure 1b is taken to be a paraboloid of revolution.[2,3] In this case, the intensity just inside the top surface of the LC (that is, below the solar cell in Figure 1b) is evaluated numerically via ray-tracing for an azimuthally symmetric emission cone filling the same [44°, 56°] polar angle wedge. The resulting intensity distribution is shown in Figure 1c, normalized relative to the intensity detected within a vertically oriented plane in the same LC with no nonimaging optic as in Figure 1a. The average intensity enhancement within the square cell area of side length $d_{cell} = d_{LC}(\tan\theta_2 - \tan\theta_1)$ is found to be $\beta_{3D} = 5.1$, which is smaller than the ideal extension of the 2D result, $(\beta_{2D})^2 = 15$, owing to skew rays that are not collected by the 3D nonimaging optic (that is, the intensity increase beyond the cell area).[2,3]

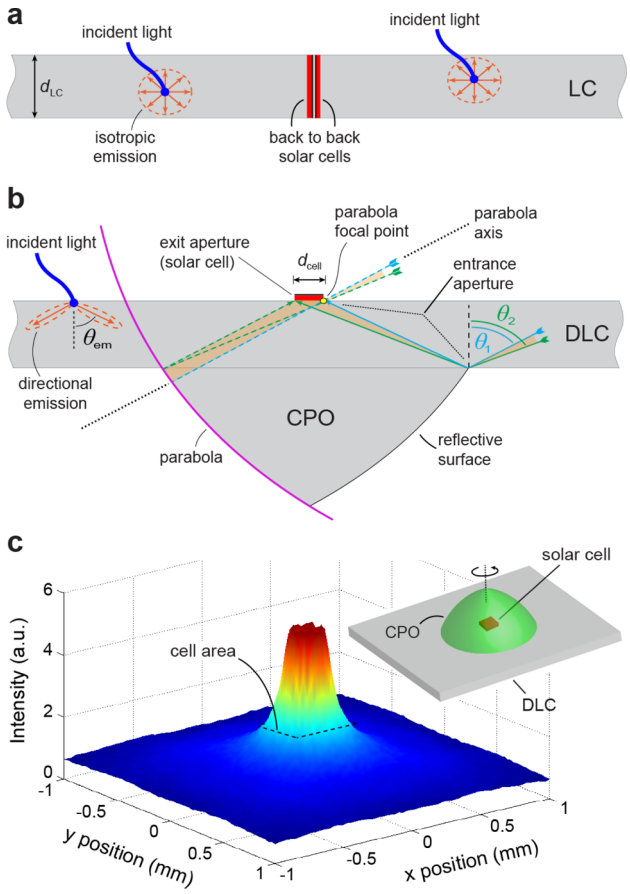

Figure 1. (a) Schematic of a conventional luminescent concentrator (LC) with isotropic emission and back-to-back photovoltaic cells to collect waveguided luminescence incident from both directions. (b) Schematic of a directional luminescent concentrator (DLC) with a "v" shaped emission profile peaked at θ_{em} within the angular interval $[\theta_1, \theta_2]$. A reflective nonimaging optic (CPO) constructed from opposing parabolas (axes tilted at θ_1) using the edge ray principle ensures that all waveguided luminescence is redirected to the surface-mounted solar cell. (c) Simulated luminescent intensity distribution at the DLC surface (in contact with the photovoltaic cell) for a three-dimensional CPO of revolution as depicted in the inset. Luminescence is emitted within the quasi-infinite DLC uniformly in an azimuthally symmetric, conical emission profile in the polar angle interval [44°, 56°]. The resulting intensity distribution is normalized to that recorded with no CPO in the DLC vertical plane as in (a) and demonstrates a geometric intensity enhancement of 5.1× averaged over the square solar cell area indicated by the dashed line.

EVANESCENTLY COUPLED DLC EMISSION

Various approaches have been demonstrated to manipulate the rate and directionality of spontaneous emission by engineering the photon density of states using microcavities, surface plasmon modes, optical antennas, and dispersion-engineered metamaterials,[23−27] as well as by simply aligning the emissive transition dipole moments.[28,29] However, because most LC applications are predicated on the basis of low cost, any means to impart emission directionality in a DLC should be simple, inexpensive, scalable, and low loss, that is, the structure cannot introduce nonradiative pathways that quench or absorb emission, which effectively rules out the use of metal.

dx.doi.org/10.1021/ph500196r | ACS Photonics 2014, 1, 746−753

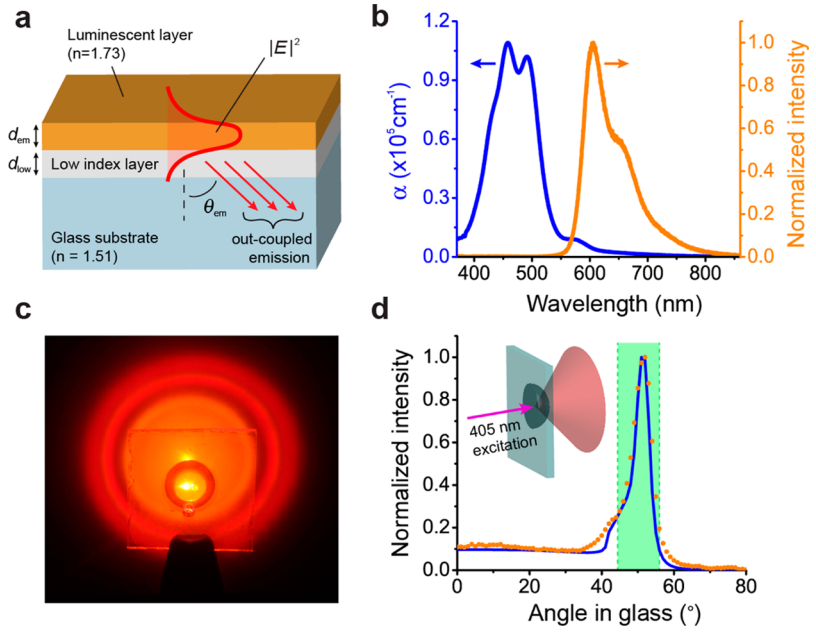

Figure 2. (a) Structure of the bilayer film used to achieve directional emission. Luminescence is emitted predominantly into a discrete waveguide mode of the luminescent layer illustrated via its optical field intensity profile ($|E|^2$). When the low refractive index layer is less than the order of a wavelength, the mode evanescently overlaps with the substrate and can become leaky, coupling power out at a sharply defined angle (θ_{em}) that corresponds to the modal propagation constant. (b) Absorption coefficient and photoluminescence spectrum of a Lumogen thin film consisting of an L083 host coevaporated with 2 wt % L305. Absorption is dominated by L083 (λ < 550 nm; the small shoulder near $\lambda \sim 580$ nm is due to L305) whereas emission occurs solely from L305 owing to efficient host → guest Förster energy transfer. (c) Photograph of the conical emission profile from a typical bilayer (d_{em} = 81 nm, d_{low} = 290 nm) out-coupled with a half-ball lens as in the inset of (d) and projected on a white card. (d) Angular intensity distribution measured for the same sample together with that predicted from transfer matrix simulation (solid line). The green shaded region indicates the angular range targeted for nonimaging gain.

The evanescently coupled bilayer DLC strategy introduced in ref 30 has the potential to satisfy these constraints. As outlined in Figure 2a, this approach involves a luminescent thin film waveguide separated from a glass or acrylic substrate by a low refractive index (low-n) layer. In this arrangement, the emissive layer thickness (d_{em}) is designed to support a single leaky waveguide mode that evanescently couples power into the substrate at a well-defined angle corresponding to its discrete propagation constant. Because the guided mode constitutes a peak in the k-space photon density of states in the luminescent film, the majority of spontaneous emission couples into it, thereby resulting in a conical emission profile sharply peaked at a particular polar angle, θ_{em}, as sketched in Figure 2a.

To ensure single mode operation and thus maximize emission directionality (that is, emission in only one cone), d_{em} is limited to approximately half the emission wavelength ($\lambda_{em}/2$) and thus the luminescent layer must absorb strongly above its optical gap with absorption coefficient $\alpha > 1/d_{em} \sim 10^5$ cm^{-1}. As demonstrated previously,[31] the needed combination of strong absorption and high photoluminescence quantum yield (PLQY) can be achieved with composite small molecule thin films that exploit host → guest Förster energy transfer to reduce self-absorption overlap and prevent self-quenching among guest dye molecules. The same strategy is adopted here using L083 Yellow and L305 Red Lumogen-F dyes available from BASF Inc., which are commonly used in LCs owing to their strong absorption, environmental stability, and high PLQY.[13]

To avoid the aggregation-induced red-shift and self-quenching that occurs for each dye in neat film, we use the pair in a coevaporated guest−host composite consisting of 2 wt % L305 in L083. As shown in Figure 2b, absorption of the composite is dominated by the L083 host with α peaking >10^5 cm^{-1}, whereas quantitative L083 → L305 Förster transfer results in emission solely from the L305 guest with a net PLQY = 0.29 ± 0.03.[32] The L305 concentration used here represents a compromise between that needed to maintain complete energy transfer (that is, average L305 spacing less than the L083-L305 Förster radius) and that desired to minimize self-quenching, where PLQY ≈ 1 at low concentration <10^{-3} wt %.[33] Aside from its suboptimal PLQY, this composite meets the basic criteria for a DLC emitter and is highly stable in air under illumination (no change in PLQY was observed throughout testing), making it a reasonable starting point to investigate nonimaging DLC enhancement.

The photograph in Figure 2c shows the conical emission out-coupled from a DLC bilayer using a half-ball lens as depicted in the inset of Figure 2d. The emissive and low-n film thicknesses (d_{em} = 81 ± 3 nm and d_{low} = 290 ± 10 nm, respectively) are chosen to support only the lowest order transverse electric (TE_0) mode with a propagation constant tuned for leakage into the glass substrate at θ_{em} = 53°, as shown in Figure 2d. There, 63% of the emission lies within the [44°, 56°] angular range (green shaded area) whereas integrating sphere measurements indicate 68 ± 4% of all emitted light is coupled into the glass beyond the critical angle (see Supporting Information, Figure S1). This is comparable to the fraction of isotropic emission confined by total internal reflection in conventional LCs (~74%)[8] and therefore demonstrates that efficient DLC emission can be achieved in a reasonable approximation to that targeted for nonimaging gain in the context of Figure 1b,c.

dx.doi.org/10.1021/ph500196r | ACS Photonics 2014, 1, 746−753

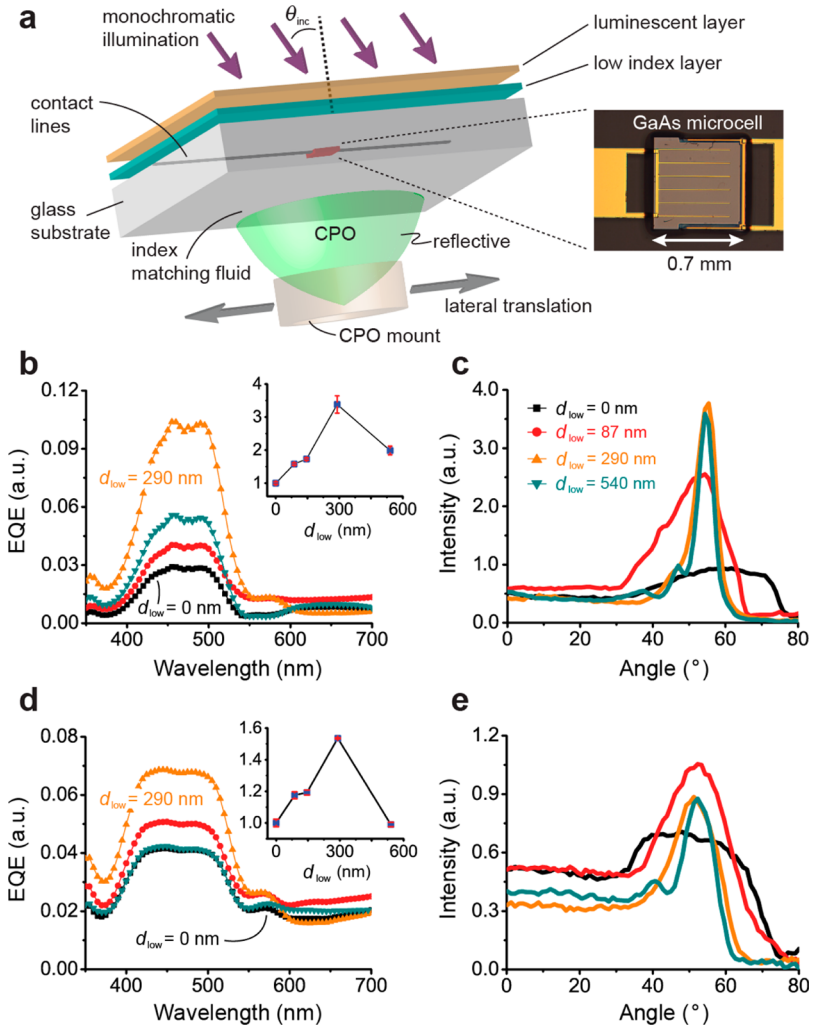

Figure 3. (a) Exploded view of the experimental test setup. The GaAs microcell photovoltaic shown in the inset micrograph is transfer-printed onto the DLC glass substrate beneath the luminescent/low index bilayer; these layers are artificially spaced from one another in the diagram for clarity. The compound parabolic optic (CPO) is coupled to the glass with index matching fluid and is held by a mount fixed to crossed translation stages that enable precise control of its lateral position relative to the microcell. (b) Relative external quantum efficiency (EQE) measured for a series of samples with d_{em} = 81 nm and varying low index layer thickness d_{low} = 0, 87, 290, and 540 nm. The inset plots the EQE integrated over the [350, 600] nm wavelength interval normalized to that of the conventional LC reference including the CPO (d_{low} = 0 nm, black squares); the EQE is lower for the LC or any of the DLCs without the CPO (not shown). (c) Corresponding angular emission profiles measured for the different samples, demonstrating a directional emission peak that emerges and sharpens at $\theta_{em} \sim 53°$ with increasing low-n layer thickness. (d, e) Analogous data obtained for samples with a thicker emissive layer, d_{em} = 370 nm to ensure complete absorption. The nonimaging DLC enhancement in this case is lower than in (b) due to decreased emission directionality and reduced out-coupling as discussed in the text.

NONIMAGING DIRECTIONAL LC ENHANCEMENT WITH MICROCELL PHOTOVOLTAICS

To test the predictions of Figure 1, a custom compound paraboloidal optic (CPO) was turned from acrylic plastic and integrated together with a DLC and a microscale (0.7 × 0.7 mm^2) GaAs photovoltaic cell,[34,35] as depicted in Figure 3a. The CPO is coated with a 200 nm thick reflective Ag layer and coupled to the substrate side of the DLC with index matching fluid that allows its lateral position relative to the microcell to be controlled via a pair of crossed translation stages (see Supporting Information, Figure S2 for details). External quantum efficiency (EQE) spectra were subsequently collected under monochromatic illumination using synchronous lock-in detection at different incidence angles (θ_{inc}), indicated in Figure 3a.

Figure 3b shows the EQE data obtained at $\theta_{inc} = 25°$ for a series of samples with fixed emissive layer thickness (d_{em} = 81 nm) and varying low-n layer thickness, d_{low} = 0 nm (that is, no low-n layer), 87, 290, and 540 nm. As compared to the conventional LC (d_{low} = 0 nm) with or without the CPO, there is a significant boost in DLC EQE over the L083 absorption band ($350 < \lambda < 600$ nm) that grows significantly with increasing low-n layer thickness and peaks at d_{low} = 290 nm. This improvement is quantified in the inset of Figure 3b and stems directly from the narrowing DLC angular emission profile shown in Figure 3c, which evolves from unstructured emission when d_{low} = 0 nm to a sharply peaked distribution at $\theta_{em} \sim 53°$ when $d_{low} \geq 290$ nm, thereby better exploiting the [44°, 56°] acceptance interval of the CPO.

This trend is understood from the decreasing modal resonance width expected upon increasing d_{low} due to the associated decrease in radiative damping (that is, smaller imaginary component of the modal propagation constant and thus longer propagation length for evanescent out-cou-

dx.doi.org/10.1021/ph500196r | ACS Photonics 2014, 1, 746−753

pling).[36,37] Outside of evanescent out-coupling, which depends exponentially on d_{low}, the resonance width is ultimately limited by parasitic scattering loss from surface roughness/imperfections, intrinsic material loss (due here to self-absorption from the small L305 Stokes' shift), and most significantly in this case, chromatic modal dispersion over the broad L305 emission spectrum. Consequently, the DLC angular width ($\Delta\theta_{em}$) asymptotes to a minimum with increasing d_{low} as the substrate coupling decreases to the level of the underlying self-absorption and scattering loss, at which point these processes dominate the modal power dissipation and the emission yield into the substrate decreases. There is thus an optimum low-n thickness that maximizes directionality while maintaining efficient luminescence extraction into the substrate. This point is evident in Figure 3b,d, where increasing d_{low} from 290 to 540 nm does not further improve the emission directionality but does lead to a substantial decrease in EQE as out-coupling into the substrate becomes inefficient.

At an emissive layer thickness of 81 nm, single pass absorption within the L083 absorption band is only ∼50% (see Supporting Information, Figure S3). Although this could be improved with the addition of a backside reflector,[35,38] it is nevertheless desirable to operate with a thicker luminescent layer that ensures complete absorption. Figure 3d and 3e, respectively, present the EQE and angular emission profile measured for DLCs with d_{em} = 370 nm (>3 absorption lengths) designed for emission into the TE_1 mode while maintaining θ_{em} ≈ 53°. A similar EQE trend is observed with increasing d_{low} as in Figure 3b, however the enhancement is lower in this case (factor of ∼1.5) due to reduced substrate out-coupling and directional broadening of the DLC emission (cf, Figure 3e) outside of the [44°, 56°] CPO acceptance range. Both effects stem primarily from increased self-absorption loss in the luminescent layer owing to a ∼1.7× increase in modal confinement factor (see Supporting Information, Figure S4) and could therefore be mitigated by exploiting a phosphorescent guest or other terminal dyes that have a larger Stokes' shift than L305.[13,31]

Figure 4 explores the impact of directionality on nonimaging gain in more detail by mapping short-circuit current under illumination at the L083 absorption peak (λ = 470 nm) as a function of lateral misalignment between the CPO and the microcell. Figure 4a displays the result for the d_{em} = 81 nm, d_{low} = 290 nm DLC from Figure 3b, which indicates that the luminescent intensity distribution is strongly peaked, in contrast to the same measurement performed on the corresponding d_{em} = 81 nm conventional LC (including the CPO), which exhibited no spatial intensity variation (not shown). Normalizing the data in Figure 4a to the conventional LC photocurrent for comparison, these results confirm that geometric concentration is the basis for the 3-fold EQE enhancement observed in Figure 3b. The measured DLC photocurrent map is qualitatively reproduced in Figure 4b by convolving the microcell area with the luminescent intensity distribution simulated via ray-tracing from the associated angular emission profile in Figure 3c.

Progressing toward a CPO/microcell array for a large area DLC panel, Figure 5a examines how the power delivered to the microcell from Figure 4a depends on illumination area (that is, the geometric gain). There, the DLC power exhibits rapid initial growth at small illumination diameter since the majority of luminescence is emitted near the center of the CPO and therefore naturally interacts with it on axis (that is, in-plane ray

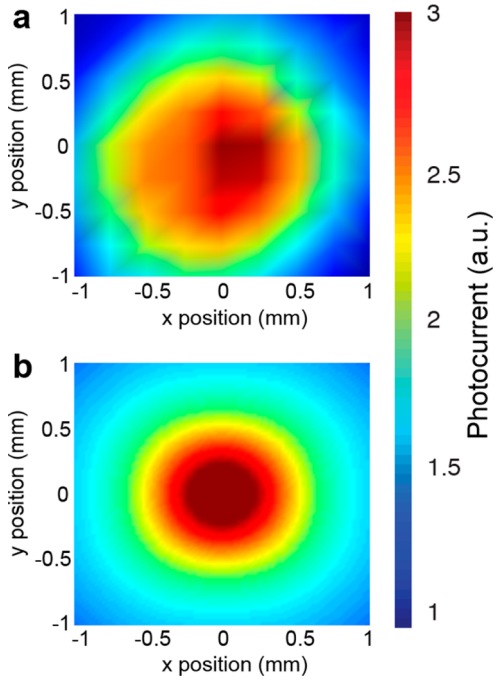

Figure 4. (a) Map of the microcell short-circuit current as a function of lateral misalignment between it and the center of the CPO mounted on a DLC (d_{low} = 290 nm, d_{em} = 81 nm) under λ = 470 nm illumination. Shading reflects interpolation from the original 9 × 9 grid of data points. The photocurrent is normalized to the average value of an analogous plot collected for the corresponding conventional LC (d_{low} = 0 nm, d_{em} = 81 nm), which exhibited no spatial variation in intensity (not shown). The peak at the origin observed here for the DLC confirms nonimaging geometric gain as the source of the EQE enhancement observed in Figure 3b. (b) Simulation of the DLC photocurrent map in (a) obtained by convolving the microcell area together with the luminescent intensity distribution derived from ray tracing.

trajectories parallel to the CPO radius vector) for optimum geometric concentration. As the illumination spot exceeds the area covered by the CPO, the rate of increase slows and ultimately becomes comparable to that of the conventional LC control as more and more of the added luminescence reaches the CPO off-axis and is rejected back into the waveguide.

Interestingly, off-axis skew luminescence rejected by one CPO can be recovered by a neighbor, resulting in a cooperative ray-recycling effect[22] that makes the geometric gain of a DLC array greater than the sum of its parts. This effect is demonstrated in Figure 5b, where the power delivered to a single CPO/microcell "probe" in a quasi-infinite, hexagonally tiled DLC panel is simulated as a function of the array lattice constant, a_0. In the large lattice constant limit, the probe power approaches that for a lone CPO/microcell (blue dashed line), whereas at small a_0 comparable to the CPO diameter, the power received by any given microcell decreases due to shadowing by its neighbors. The shadowing interaction is incomplete, however, since it is possible for skew rays rejected by one CPO to be collected on-axis by another as depicted in the inset.

This recycling effect is significant. Eliminating the exchange of light among CPOs by making them (that is, those surrounding the probe) perfectly absorptive leads to a drop in probe power (orange line). The balance therefore represents the ray-recycling contribution (highlighted gray region) and

dx.doi.org/10.1021/ph500196r | ACS Photonics 2014, 1, 746−753

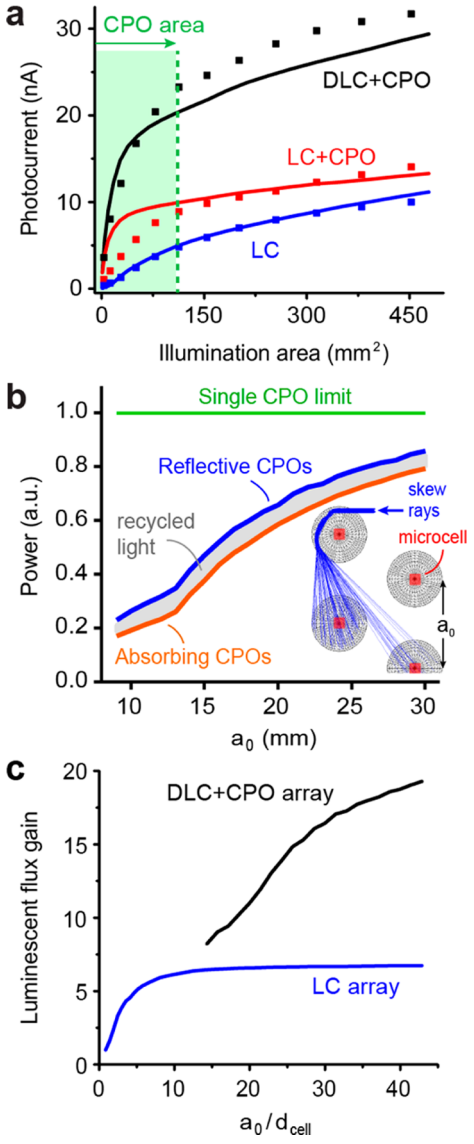

Figure 5. (a) Microcell photocurrent measured using a DLC (d_{low} = 290 nm, d_{em} = 81 nm) and its conventional LC reference (d_{low} = 0 nm) with and without the CPO as a function of the illuminating spot area (λ_{inc} = 470 nm). The DLC current increases rapidly relative to the LC when the illumination underfills the CPO area (shaded region) and the majority of emission interacts with the CPO on axis where nonimaging gain is maximum. Solid lines indicate the corresponding photocurrents predicted from ray-tracing simulation. (b) Simulation of the power received by a single "probe" microcell [using the same parameters as in (a)] within a hexagonally tiled panel as a function of the lattice constant a_0 when the surrounding CPOs are reflective (blue line) and absorptive (orange line). The difference (shaded region) marks the contribution of recycled luminescence rejected by the surrounding CPOs and collected by the probe as illustrated schematically in the inset ray-tracing diagram (top view). In the limit of large lattice constant, the probe power approaches that of a lone CPO/microcell pair (green line) as shading by the others becomes negligible. (c) Luminescent flux gain calculated for the same panel compared with that for a conventional LC with no CPOs. The conventional LC microcell array saturates at small lattice constant since shading between neighbors quickly becomes negligible. Starting from a close-packed configuration, the DLC + CPO panel grows to enable a >2.8× increase in power delivered to each microcell.

indicates that this cooperative effect improves light collection by up to ~20% in dense hexagonal CPO/microcell arrays. Figure 5c subsequently places the performance of this DLC panel in context with its conventional counterpart (without CPOs), demonstrating >2.8× increase in luminescent flux gain (defined as the ratio of luminescent irradiance incident on the microcell surface relative to that emitted from the panel surface) due entirely to secondary geometric concentration. The luminescent flux gain is plotted here because it is independent of the luminescent layer absorption and PLQY and therefore enables comparison of the secondary geometric gain among different LC architectures independent of material platform.

For the L083/L305 composite used here and the microcell array implementation in Figure 5c at a_0/d_{cell} = 40, we estimate the absolute concentration ratio, defined as the ratio of luminescent irradiance incident on the microcell surface to the solar irradiance incident on the concentrator surface above the solar cell bandgap to be CR = 0.5 and 1.5 for the conventional LC and DLC, respectively. The corresponding optical efficiencies are 0.03 and 0.1% owing to the high geometric gain ($G = \sqrt{3}a_0^2/2d_{cell}^2 = 1385$) dictated by our microcell-based experimental implementation. It is important to note, however, that the secondary geometric intensity increase (β) derived above is scale invariant and is therefore equally applicable at smaller $G < 20$ where optical efficiency is much higher.

While the surface-mounted CPO implementation for DLC nonimaging concentration is convenient for experimental demonstration, even the ideal 2D solution outlined in Figure 1b falls short of the thermodynamic limit since the input angular extent $\Delta\theta_{em}$ is only transformed into the interval $[-\theta_{em}, \theta_{em}]$ instead of the full 180° half-space.[1,2] An interesting consequence of this is that the CPO also directly concentrates a portion of normally incident light not absorbed by the luminescent layer (for example, below the absorption optical gap) as detailed in Supporting Information, Figure S5. The limiting geometric intensity enhancement for directional luminescence within the angular wedge $[\theta_1, \theta_2]$ in Figure 1b can nevertheless be found from sine law consideration as $\beta_{2D,lim} = [\sin(\theta_2) - \sin(\theta_1)]^{-1}$, which is nearly double that of the surface-mounted CPO for the [44°, 56°] interval considered here.

Alternative nonimaging solutions that ideally exploit high angle emission ($\beta_{2D,lim}$ maximizes for $\theta_{em} \rightarrow 90°$) such as, for example, edge-mounted implementations, are thus likely to enable further improvement in geometric gain. More broadly, however, the challenge to fully harness the power of nonimaging optics in luminescent concentration lies in globally optimizing the emission profile and optical design together. While the emission directionality (that is, $\Delta\theta_{em}$) of the present bilayer DLC can be improved by reducing self-absorption and choosing a narrow spectral bandwidth emitter (for example, phosphorescent molecules, rare-earth complexes or quantum dots),[13,31,39−42] the unconstrained azimuthal degree of freedom inherent in any layered thin film DLC photonic structure presents a fundamental challenge for maximum nonimaging concentration.

Exploring the extent to which collective interaction among discrete optics (for example, ray-recycling) can be leveraged to function as a single (distributed) nonimaging element provides one route; however, the task will be greatly simplified by imposing azimuthal emission control. This could be accomplished by embossing or stamping in-plane photonic structure

dx.doi.org/10.1021/ph500196r | ACS Photonics 2014, 1, 746−753

such as grating/photonic crystal patterns into the emissive layer[43,44] or alternatively by aligning the transition dipole moment of emissive dye molecules.[28,29] Paramount for any such effort, however, is that the result be inexpensive, robust, and scalable.

CONCLUSION

In conclusion, we have established a path to leverage nonimaging optics in luminescent concentration by controlling the directionality of emitted light and have demonstrated that it enables a 3-fold increase in luminescent concentration ratio for surface-mounted photovoltaic cells. In addition to photovoltaics, we expect this development will also prove useful for other applications such as scintillator-based radiation detection, where directional emission from a wavelength-shifting film applied to the surface of a scintillator plate could enable substantial improvement in luminescence collection and overall system sensitivity.

METHODS

Modeling. Transfer matrix modeling based on the method of source terms[45,46] was used to predict the angular emission profile, power dissipation, and optical out-coupling fraction of DLC bilayers. These data were used as the source input for nonsequential ray tracing simulations carried out using Zemax commercial software[47] with $>10^6$ rays employed for run-to-run variation of less than 0.3%. All optical constants, polarization-dependent Fresnel reflections, and thin film interference effects are accounted for.

Sample Fabrication. Lumogen dyes were obtained from BASF Inc. and subsequently purified via thermal gradient sublimation. LC and DLC emitters were fabricated on borosilicate glass microscope coverslips (25 mm × 25 mm, 0.17 mm thick, Fisher Scientific), spin-coating the low-n layer as described previously.[48] Host−guest L083/L305 emissive layer films were deposited via thermal coevaporation from a base pressure of 2.0×10^{-7} Torr using computer-controlled independent quartz crystal microbalances for rate/thickness control. The optical constant dispersions for the L083/L305 and low-n films are provided in Supporting Information, Figure S6. The microscale photovoltaic cell is grown via metal−organic chemical vapor deposition and consists of a vertical GaAs pn junction with 700 μm × 700 μm square lateral dimensions and a thickness of 3 μm. Lithographically defined microcells are released by selective etching of an $Al_{0.95}Ga_{0.05}As$ sacrificial layer and then individually bonded onto glass support substrates (0.15 mm thick) by transfer printing.[35,49] Metallic contact lines made of Cr/Cu/Au (10 nm/500 nm/10 nm) are used for electrical interconnection.

The CPO was designed in Zemax and diamond-turned from acrylic plastic (Nanophorm, LLC) followed by evaporation of a 200 nm thick reflective Ag coating onto its revolved surface. The base of the CPO was coupled to the underside of a 1 mm thick glass support slide with index-matching fluid (n = 1.517, Cargille Laboratories) and seated in a cylindrical holder attached to a pair of crossed translation stages to precisely control its position. The coverslip holding the microcell was subsequently index-matched to the top surface of the support glass (cell facing down toward the CPO) followed by the DLC-coated coverslip (luminescent layer facing up) to create a single DLC/microcell/CPO system with no optical discontinuity; Supporting Information, Figure S2 provides a detailed schematic of the sample and experimental setup.

Measurements and Data Analysis. Optical constant dispersions of the low-n and luminescent films were measured using variable angle spectroscopic ellipsometry. LC and DLC photoluminescence quantum yields were measured using an integrating sphere under λ = 355 nm excitation with a cooled CCD spectrograph.[32] Angular emission profiles were collected by out-coupling luminescence from the glass substrate with an index-matched 10 mm diameter half-ball lens and recording it with a Si photodiode mounted on an automated rotation stage to achieve an angular resolution <0.2°. Spatially uniform, monochromatic (5 nm bandwidth) illumination was obtained from a laser-driven Xe light source (Energetiq) coupled through a 1/8 m monochromator using all-reflective optics to prevent chromatic dispersion. Samples were illuminated from above in a circular spot (see Supporting Information, Figure 2a) with 25 mm diameter, except in Figure 5a where the area was varied with an iris. External quantum efficiency spectra were collected synchronously with a lock-in amplifier at a chopping frequency of 2 kHz under short-circuit conditions.

ASSOCIATED CONTENT

Supporting Information

Supporting material contains additional details on the construction of the CPO, the experimental method used to test it with the different luminescent concentrators, and their performance as a function of incidence angle. Refractive index dispersions and transmission spectra of the LC and DLC films are also included, together with the measurement of their luminescence quantum yields. This material is available free of charge via the Internet at http://pubs.acs.org.

AUTHOR INFORMATION

Corresponding Author

*E-mail: ncg2@psu.edu.

Notes

The authors declare no competing financial interest.

ACKNOWLEDGMENTS

This work was supported in part by the DARPA Young Faculty Award and the DOE SunShot program under Award No. DE-EE0005798. X.S. and J.A.R. acknowledge support from the DOE "Light-Material Interactions in Energy Conversion" Energy Frontier Research Center under Grant DE-SC0001293. L.S. acknowledges support from the China Scholarship Council.

REFERENCES

(1) Welford, W. T.; Winston, R. *High Collection Non-Imaging Optics*; Academic Press: New York, 1989.
(2) Winston, R.; Miñano, C. J.; Benitez, P. *Nonimaging Optics*; Academic Press: New York, 2005.
(3) O'Gallagher, J. J. *Nonimaging Optics in Solar Energy*; Morgan & Claypool: San Rafael, CA, 2008.
(4) Hinterberger, H.; Winston, R. Efficient Light Coupler for Threshold Cerenkov Counters. *Rev. Sci. Instrum.* **1966**, *37*, 1094.
(5) Smestad, G.; Ries, H.; Winston, R.; Yablonovitch, E. The Thermodynamic Limits of Light Concentrators. *Sol. Energy Mater.* **1990**, *21*, 99−111.
(6) Yablonovitch, E. Thermodynamics of the Fluorescent Planar Concentrator. *J. Opt. Soc. Am.* **1980**, *70*, 1362−1363.

(7) Debije, M. G.; Verbunt, P. P. C. Thirty Years of Luminescent Solar Concentrator Research: Solar Energy for the Built Environment. *Adv. Energy Mater.* **2011**, *2*, 12−35.
(8) Batchelder, J. S.; Zewail, A. H.; Cole, T. Luminescent Solar Concentrators 0.1. Theory of Operation and Techniques for Performance Evaluation. *Appl. Opt.* **1979**, *18*, 3090−3110.
(9) Goetzberger, A. Fluorescent Solar Energy Concentrators: Principle and Present State of Development. In *High-Efficient Low-Cost Photovoltaics: Recent Developments*; Petrova-Koch, V. H. R. G. A., Ed.; Springer: New York, 2009; Vol. *140*, pp 159−176.
(10) Olson, R. W.; Loring, R. F.; Fayer, M. D. Luminescent Solar Concentrators and the Reabsorption Problem. *Appl. Opt.* **1981**, *20*, 2934−2940.
(11) Roncali, J.; Garnier, F. Photon-Transport Properties of Luminescent Solar Concentrators - Analysis and Optimization. *Appl. Opt.* **1984**, *23*, 2809−2817.
(12) Debije, M. G.; Verbunt, P. P. C.; Rowan, B. C.; Richards, B. S.; Hoeks, T. L. Measured Surface Loss from Luminescent Solar Concentrator Waveguides. *Appl. Opt.* **2008**, *47*, 6763−6768.
(13) Rowan, B. C.; Wilson, L. R.; Richards, B. S. Advanced Material Concepts for Luminescent Solar Concentrators. *IEEE J. Sel. Top. Quant.* **2008**, *14*, 1312−1322.
(14) Farrell, D. J.; Yoshida, M. Operating Regimes for Second Generation Luminescent Solar Concentrators. *Prog. Photovolt: Res. Appl.* **2011**, *20*, 93.
(15) Rowan, B.; Mc Cormack, S.; Doran, J.; Norton, B. Quantum dot solar concentrators: An investigation of various geometries - art. no. 66490A. In *High and Low Concentration for Solar Electric Applications II*; SymkoDavies, M., Ed.; Society of Photo Optical: Bellingham, WA, 2007; Vol. *6649*, pp A6490−A6490.
(16) Edelenbosch, O. Y.; Fisher, M.; Patrignani, L.; van Sark, W. G. J. H. M.; Chatten, A. J. Luminescent Solar Concentrators with Fiber Geometry. *Opt. Express* **2013**, *21*, A503−A514.
(17) Debije, M. G.; Van, M. P.; Verbunt, P. P. C.; Kastelijn, M. J.; van der Blom, R. H. L.; Broer, D. J.; Bastiaansen, C. W. M. Effect on the Output of a Luminescent Solar Concentrator on Application of Organic Wavelength-Selective Mirrors. *Appl. Opt.* **2010**, *49*, 745−751.
(18) Peters, M.; Goldschmidt, J. C.; Loper, P.; Blasi, B.; Gombert, A. The Effect of Photonic Structures on the Light Guiding Efficiency of Fluorescent Concentrators. *J. Appl. Phys.* **2009**, *105*, 014909.
(19) Tsoi, S.; Broer, D. J.; Bastiaansen, C. W. M.; Debije, M. G. Patterned Dye Structures Limit Reabsorption in Luminescent Solar Concentrators. *Opt. Express* **2010**, *18*, A536−A543.
(20) Tsoi, S.; Broer, D. J.; Bastiaansen, C. W. M.; Debije, M. G. Using Lenses to Improve the Output of a Patterned Luminescent Solar Concentrator. *Adv. Energy Mater.* **2013**, *3*, 337−341.
(21) Goetzberger, A.; Schirmer, O. Second-Stage Concentration with Tapers for Fluorescent Solar Collectors. *Appl. Phys.* **1979**, *19*, 53−58.
(22) Markman, B. D.; Ranade, R. R.; Giebink, N. C. Nonimaging Optics in Luminescent Solar Concentration. *Opt. Express* **2012**, *20*, A622−A629.
(23) Noda, S.; Fujita, M.; Asano, T. Spontaneous-Emission Control by Photonic Crystals and Nanocavities. *Nat. Photonics* **2007**, *1*, 449−458.
(24) Noginov, M. A.; Li, H.; Barnakov, Y. A.; Dryden, D.; Nataraj, G.; Zhu, G.; Bonner, C. E.; Mayy, M.; Jacob, Z.; Narimanov, E. E. Controlling Spontaneous Emission with Metamaterials. *Opt. Lett.* **2010**, *35*, 1863−1865.
(25) Rogobete, L.; Kaminski, F.; Agio, M.; Sandoghdar, V. Design of Plasmonic Nanoantennae for Enhancing Spontaneous Emission. *Opt. Lett.* **2007**, *32*, 1623−1625.
(26) Lalanne, P.; Hugonin, J. P. Very Large Spontaneous-Emission β Factors in Photonic-Crystal Waveguides. *Phys. Rev. Lett.* **2007**, *99*, 023902.
(27) Gutmann, J.; Zappe, H.; Goldschmidt, J. C. Quantitative Modeling of Fluorescent Emission in Photonic Crystals. *Phys. Rev. B* **2013**, *88*, 205118.
(28) Verbunt, P. P. C.; Kaiser, A.; Hermans, K.; Bastiaansen, C. W. M.; Broer, D. J.; Debije, M. G. Controlling Light Emission in Luminescent Solar Concentrators Through Use of Dye Molecules Aligned in a Planar Manner by Liquid Crystals. *Adv. Funct. Mater.* **2009**, *19*, 2714−2719.
(29) Mulder, C. L.; Reusswig, P. D.; Beyler, A. P.; Kim, H.; Rotschild, C.; Baldo, M. A. Dye Alignment in Luminescent Solar Concentrators: II. Horizontal Alignment for Energy Harvesting in Linear Polarizers. *Opt. Express* **2010**, *18*, A91−A99.
(30) Giebink, N. C.; Wiederrecht, G. P.; Wasielewski, M. R. Resonance-Shifting to Circumvent Reabsorption Loss in Luminescent Solar Concentrators. *Nat. Photonics* **2011**, *5*, 695−702.
(31) Currie, M. J.; Mapel, J. K.; Heidel, T. D.; Goffri, S.; Baldo, M. A. High-Efficiency Organic Solar Concentrators for Photovoltaics. *Science* **2008**, *321*, 226−228.
(32) deMello, J. C.; Wittmann, H. F.; Friend, R. H. An Improved Experimental Determination of External Photoluminescence Quantum Efficiency. *Adv. Mater.* **1997**, *9*, 230−&.
(33) Wilson, L. R.; Richards, B. S. Measurement Method for Photoluminescent Quantum Yields of Fluorescent Organic Dyes in Polymethyl Methacrylate for Luminescent Solar Concentrators. *Appl. Opt.* **2009**, *48*, 212−220.
(34) Yoon, J.; Jo, S.; Chun, I. S.; Jung, I.; Kim, H.-S.; Meitl, M.; Menard, E.; Li, X.; Coleman, J. J.; Paik, U.; Rogers, J. A. GaAs Photovoltaics and Optoelectronics Using Releasable Multilayer Epitaxial Assemblies. *Nature* **2010**, *465*, 329−U80.
(35) Sheng, X.; Shen, L.; Kim, T.; Li, L.; Wang, X.; Dowdy, R.; Froeter, P.; Shigeta, K.; Li, X.; Nuzzo, R. G.; Giebink, N. C.; Rogers, J. A. Doubling the Power Output of Bifacial Thin-Film GaAs Solar Cells by Embedding Them in Luminescent Waveguides. *Adv. Energy Mater.* **2013**, *3*, 991−996.
(36) Reisinger, A. Characteristics of Optical Guided Modes in Lossy Waveguides. *Appl. Opt.* **1973**, *12*, 1015−1025.
(37) Hu, J.; Menyuk, C. R. Understanding Leaky Modes: Slab Waveguide Revisited. *Adv. Opt. Photonics* **2009**, *1*, 58−106.
(38) Slooff, L. H.; Bende, E. E.; Burgers, A. R.; Budel, T.; Pravettoni, M.; Kenny, R. P.; Dunlop, E. D.; Buchtemann, A. A Luminescent Solar Concentrator with 7.1% Power Conversion Efficiency. *Phys. Status Solidi RRL* **2008**, *2*, 257−259.
(39) Meinardi, F.; Colombo, A.; Velizhanin, K. A.; Simonutti, R.; Lorenzon, M.; Beverina, L.; Viswanatha, R.; Klimov, V. I.; Brovelli, S. Large-Area Luminescent Solar Concentrators Based on Stokes-Shift-Engineered Nanocrystals in a Mass-Polymerized PMMA Matrix. *Nat. Photonics* **2014**, *8*, 392−399.
(40) Erickson, C. S.; Bradshaw, L. R.; McDowall, S.; Gilbertson, J. D.; Gamelin, D. R.; Patrick, D. L. Zero-Reabsorption Doped-Nanocrystal Luminescent Solar Concentrators. *ACS Nano* **2014**, *8*, 3461−3467.
(41) Bronstein, N. D.; Li, L.; Xu, L.; Yao, Y.; Ferry, V. E.; Alivisatos, A. P.; Nuzzo, R. G. Luminescent Solar Concentration with Semiconductor Nanorods and Transfer-Printed Micro-Silicon Solar Cells. *ACS Nano* **2014**, *8*, 44−53.
(42) Coropceanu, I.; Bawendi, M. G. Core/Shell Quantum Dot Based Luminescent Solar Concentrators with Reduced Reabsorption and Enhanced Efficiency. *Nano Lett.* **2014**, DOI: 10.1021/nl501627e.
(43) Rousseau, I.; Wood, V. Nanophotonic Luminescent Solar Concentrators. *Appl. Phys. Lett.* **2013**, *103*, 131113.
(44) Fehrembach, A. L.; Enoch, S.; Sentenac, A. Highly Directive Light Sources Using Two-Dimensional Photonic Crystal Slabs. *Appl. Phys. Lett.* **2001**, *79*, 4280−4282.
(45) Benisty, H.; Stanley, R.; Mayer, M. Method of Source Terms for Dipole Emission Modification in Modes of Arbitrary Planar Structures. *J. Opt. Soc. Am. A* **1998**, *15*, 1192−1201.
(46) Yeh, P. *Optical Waves in Layered Media*; Wiley: New York, 2005.
(47) Radiant Zemax, http://www.radiantzemax.com.
(48) Giebink, N. C.; Wiederrecht, G. P.; Wasielewski, M. R. Strong Exciton-Photon Coupling with Colloidal Quantum Dots in a High-Q Bilayer Microcavity. *Appl. Phys. Lett.* **2011**, *98*, 081103.
(49) Sheng, X.; Corcoran, C. J.; He, J.; Shen, L.; Kim, S.; Park, J.; Nuzzo, R. G.; Rogers, J. A. Enhanced Ultraviolet Responses in Thin-Film InGaP Solar Cells by Down-Shifting. *Phys. Chem. Chem. Phys.* **2013**, *15*, 20434−20437.